Dimensional reduction of the Luttinger Hamiltonian and g-factors of holes in symmetric two-dimensional semiconductor heterostructures

D. S. Miserev and O. P. Sushkov
School of Physics, University of New South Wales, Sydney, Australia
(Received 10 October 2016; published 23 February 2017)

The spin-orbit interaction of holes in zinc-blende semiconductors is much stronger than that of electrons. This makes the hole systems very attractive for possible spintronics applications. In three dimensions (3D), the dynamics of holes is described by well-known Luttinger Hamiltonian. However, most recent spintronics applications are related to two-dimensional (2D) heterostructures where dynamics in one direction is frozen due to quantum confinement. The confinement results in dimensional reduction of the Luttinger Hamiltonian, 3D $\rightarrow$ 2D. Due to the interplay of the spin-orbit interaction, the external magnetic field, and the lateral gate potential imposed on the heterostructure, the reduction is highly nontrivial and as yet unknown. In the present work we perform the reduction and hence derive the general effective Hamiltonian which describes spintronics effects in symmetric 2D heterostructures. In particular, we do the following: (i) derive the spin-orbit interaction and the Darwin interaction related to the lateral gate potential, (ii) determine the momentum-dependent out-of-plane g-factor, (iii) point out that there are two independent in-plane g-factors, (iv) determine momentum dependencies of the in-plane g-factors.

DOI: 10.1103/PhysRevB.95.085431

I. INTRODUCTION

The spin-orbit interaction (SOI) in cubic zinc-blende semiconductors is of topical interest because of various spintronics applications and devices. It is well understood that SO interaction is very different for the conduction band (electrons) and for the valence band (holes). Electrons in the conduction band originate from atomic s orbitals and therefore they have spin $\frac{1}{2}$. There are two SOIs for electrons: the Dresselhaus interaction [1], which is due to inversion asymmetry in bulk, and the Rashba interaction [2], which is usually due to asymmetric two-dimensional (2D) interfaces. The SO interactions are relatively weak in semiconductors with light atoms such as GaAs, and they can become significant in semiconductors with heavy atoms such as InAs and InSb [3,4].

The valence band (holes) originates from atomic $p_{3/2}$ orbitals; therefore the effective spin is $S = 3/2$, and hence the SOI quadratic in spin is possible. This SOI is always strong; even in Si it is comparable with the kinetic energy. The quadratic in spin SOI is described by the Luttinger Hamiltonian [5]. The standard Dresselhaus interaction [1] and even an additional Dresselhaus-like interaction [6] exist for holes, too. They are relatively weak in semiconductors with light atoms such as GaAs, and they become more important in semiconductors with heavy atoms such as InAs and InSb [7,8]. Nevertheless, the most important spin-orbital physics comes from the Luttinger Hamiltonian, and this is what we consider in the present work.

Most, if not all, modern hole-based spintronics devices are essentially 2D. This includes quantum point contacts (QPCs) [9–15], quantum dots [16–19], as well as heterostructures used in Shubnikov–de Haas measurements [8,20–23]. These systems are based on quantum wells. The well freezes dynamics in one direction due to quantum confinement. The confinement results in the dimensional reduction of the Luttinger Hamiltonian, 3D $\rightarrow$ 2D; only the in-plane coordinate and associated in-plane momentum $\boldsymbol{k}$ remain as dynamic variables. Due to the interplay of the spin-orbit interaction, the external magnetic field, and the lateral gate potential imposed on the heterostructure, spin dynamics of the arising 2D system is highly nontrivial. For example, for an out-of-plane magnetic field the g-factor of holes is significantly modified by the virtual three-dimensional (3D) dynamics [24–27]. The virtual 3D dynamics is even more important for response to the in-plane magnetic field [13,28]. Effects of magnetic field in some dimensionally reduced systems have been considered previously, but only in some limiting cases [13,24–29]. The spin-orbital effects related to the lateral gate potential to the best of our knowledge have been considered before only in a very specific limit related to artificial graphene [30]. In the present work we consider the most general situation with respect to both the magnetic field and the lateral gate potential. This analysis is applicable to QPCs, quantum dots, and for laterally modulated superlattices.

In the present work we derive the general two-dimensional effective Hamiltonian resulting from the dimensional reduction of the Luttinger Hamiltonian in a symmetric heterostructure. We develop a general method for the dimensional reduction valid for any symmetric heterostructure. To be specific, we present results of numerical calculations for two different types of heterostructure: (i) a parabolic quantum well, and (ii) an infinite rectangular quantum well in GaAs and InAs. In the present work we do not consider asymmetric heterostructures which necessarily generate the Rashba-type effective interaction. Such heterostructures require techniques beyond that developed in the present work. Therefore, the asymmetric case will be a subject of a separate work.

This paper is organized as follows: in Sec. II we briefly remind the very-well-known calculation of hole subbands; see, e.g., Ref. [7]. We use results of this section in the rest of the paper. In Sec. III we introduce the effective Hamiltonian as a Ginzburg–Landau-type gradient expansion over a lateral potential. Section IV addresses momentum-dependent in-plane g-factors. In Sec. V we derive the spin-orbit interaction related to the lateral potential. To do so we use the scattering

amplitude method first developed for the Breit equation in quantum electrodynamics [31]. Usage of the method allows us to find also the Darwin term in the effective Hamiltonian. Section VI addresses the momentum-dependent out-of-plane g-factor, which is the most technically involved part. Finally, we present our conclusions in Sec. VII.

II. SUBBANDS

We start this section by recalling the very-well-known description of 2D subbands which we use in subsequent sections. Noninteracting holes in bulk conventional semiconductors are described by the Luttinger Hamiltonian [5]. In this paper, we consider so-called spherical approximation to the Hamiltonian:

$$H_L = \left(\gamma_1 + \frac{5}{2}\overline{\gamma}\right)\frac{\mathbf{p}^2}{2m} - \frac{\overline{\gamma}}{m}(\mathbf{p}\cdot\mathbf{S})^2, \tag{1}$$

where [32]

$$\overline{\gamma} = \frac{2\gamma_2 + 3\gamma_3}{5}.$$

Here $\mathbf{p}$ is 3D quasimomentum; $\mathbf{S}$ is the spin $S = 3/2$; γ_1, γ_2, and γ_3 are Luttinger parameters; and m is the free-electron mass. It is known that there is also a nonspherical part of the Luttinger Hamiltonian,

$$\delta H_L = p_i p_j S_m S_n T^{(4)}_{ijmn}, \tag{2}$$

where the irreducible fourth rank tensor $T^{(4)}_{ijmn}$ depends on the orientation of the cubic lattice. The tensor is proportional to $\gamma_2 - \gamma_3$. Since in the large spin-orbit-splitting materials $\gamma_2 \approx \gamma_3$ the rotationally noninvariant part of the Hamiltonian is small and we neglect it. Of course, there are some effects that are essentially related to the rotational asymmetry [8,20,33–35] and in these cases Eq. (2) cannot be neglected. The general techniques developed in the present work can accommodate the rotational anisotropy. Nevertheless, for clarity of presentation we omit the anisotropy in the present paper.

We impose the quantum well potential $W(z)$ on the system; the Hamiltonian reads

$$H = H_L + W(z). \tag{3}$$

The well confines dynamics along the z axis, leading to 2D subbands $\varepsilon_{n,\boldsymbol{k}}$, where $\boldsymbol{k} = (k_x, k_y) = (p_x, p_y)$ is the 2D momentum, and the integer n enumerates the bands. To be specific, we present herein numerical results for parabolic and infinite rectangular quantum wells in GaAs and InAs; see Fig. 1:

$$(i):\ W(z) = \begin{cases} 0, & z \in (-d/2, d/2) \\ \infty, & \text{otherwise,} \end{cases}$$

$$(ii):\ W(z) = \frac{m\omega_z^2 z^2}{2}. \tag{4}$$

Since z confinement is very strong, the most important part of Eq. (3) comes from terms proportional to p_z^2:

$$H_0 = \left(\gamma_1 + \frac{5}{2}\overline{\gamma} - 2\overline{\gamma}S_z^2\right)\frac{p_z^2}{2m} + W(z) + \left(\gamma_1 - \frac{5}{4}\overline{\gamma} + \overline{\gamma}S_z^2\right)\frac{k^2}{2m}. \tag{5}$$

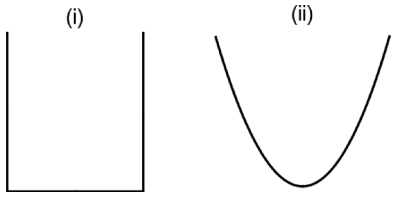

FIG. 1. Shape of quantum well: (i) infinite rectangular, (ii) parabolic.

Note that the simple in-plane kinetic energy $\propto k^2/2m$ is also included in H_0. It is evident from Eq. (5) that the lowest-energy subband comes from $S_z = \pm 3/2$. It is usually called the first "heavy hole" subband (HH1). There is also the HH2 subband, etc. The subbands with $S_z = \pm 1/2$ are called "light hole" subbands, LH1, LH2, etc. The Hamiltonian (3) can be represented as

$$H = H_0 + V,$$
$$V = -\frac{\overline{\gamma}}{4m}[k_+^2 S_-^2 + k_-^2 S_+^2 + \{p_z, k_+\}\{S_z, S_-\} + \{p_z, k_-\}\{S_z, S_+\}]. \tag{6}$$

Here, $\{\ldots\}$ denotes the anticommutator. Notice that V is off-diagonal in spin space and does not contain powers of spin higher than $S_\pm^2$. Therefore, in the leading order of perturbation theory, the HH1 doublet is coupled only with light hole states. This property is directly reflected in the structure of Eqs. (13) and (22) presented below. Evaluation and diagonalization of the Hamiltonian matrix of Eq. (6) in the basis of eigenstates of Eq. (5) is straightforward. The subbands arising from this diagonalization for GaAs and InAs are plotted in Fig. 2 for both quantum wells considered here.

Luttinger parameters used in the calculations are presented in Table I. Let us introduce the momentum unit for parabolic and rectangular wells:

$$k_0 = \begin{cases} 0.5\sqrt{m\omega_z} & \text{parabolic} \\ 2.0/d & \text{rectangular.} \end{cases} \tag{7}$$

It is useful to note that, for a rectangular quantum well with $d = 20$ nm, the Fermi momentum $k = k_0$ corresponds to the hole density 1.6×10^{11} cm^{-2}; this is about a typical experimental density. Energies we express in units

$$E_0 = \frac{\gamma_1 k_0^2}{2m}. \tag{8}$$

The energy scale for a rectangular quantum well of width $d = 20$ nm is $E_0 = 2.6$ meV which corresponds to experimental values of the Fermi energy. Effective mass $m^* = k(\frac{d\varepsilon}{dk})^{-1}$ increases with the in-plane momentum due to nonparabolic corrections; see Fig. 3.

Let us impose now a magnetic field B and a lateral potential $U(x,y)$ on the heterostructure. The magnetic field manifests itself in the long derivatives in the Hamiltonian (5), (6), $\boldsymbol{p} \to \boldsymbol{p} - e\boldsymbol{A}$, and in the Zeeman term $-2\kappa\mu_B(\boldsymbol{B}\cdot\boldsymbol{S})$. Here, $\boldsymbol{A}$ is the vector potential, e is the elementary charge, and μ_B is the Bohr magneton. Values of the material-specific parameter κ are listed in the Table I; see, e.g., Ref. [7]. Thus, the total 3D

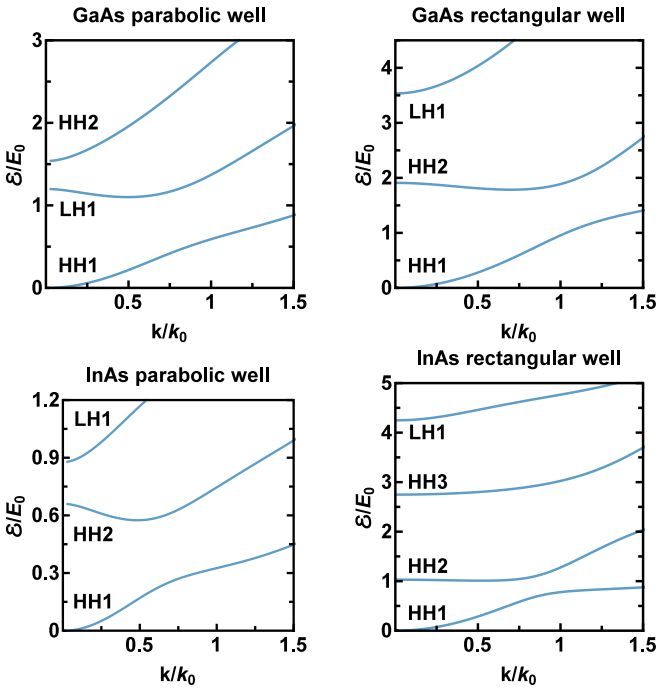

FIG. 2. Hole subbands for parabolic quantum well and for infinite rectangular well in GaAs and InAs. Momentum is given in units of k_0 [see Eq. (7)] and energy in units of E_0 [see Eq. (8)].

Hamiltonian reads

$$H = H_0(\boldsymbol{\pi}) + V(\boldsymbol{\pi}) - 2\kappa\mu_B(\boldsymbol{B}\cdot\boldsymbol{S}) + U(x,y),$$
$$\boldsymbol{\pi} = \boldsymbol{p} - e\boldsymbol{A}. \tag{9}$$

III. EFFECTIVE TWO-DIMENSIONAL HAMILTONIAN, GRADIENT EXPANSION

We consider here only HH1 subband; see Fig. 2. This implies that the Fermi energy is below the bottom of the first-excited subband. The HH1 subband is doubly degenerate due to the Kramers theorem. The standard way to describe the Kramers doublet is to introduce the effective spin $\mathbf{s} = \boldsymbol{\sigma}/2$ (pseudospin) with related Pauli matrices $\boldsymbol{\sigma}$. The correspondence at $k = 0$ is very simple, $|\uparrow\rangle = |S_z = 3/2\rangle$, $|\downarrow\rangle = |S_z = -3/2\rangle$.

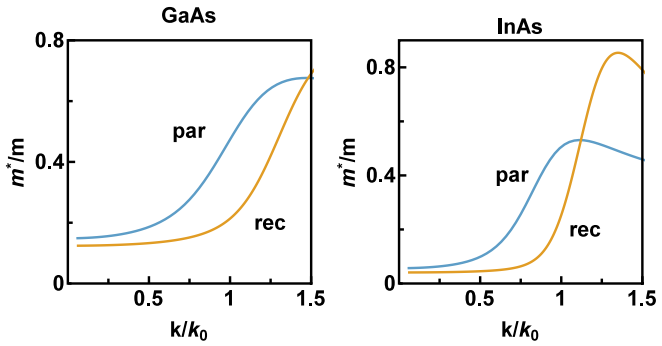

FIG. 3. The effective mass in the HH1 subband. Parabolic and rectangular quantum wells in GaAs and InAs.

TABLE I. Luttinger parameters for GaAs and InAs.

	γ_1	γ_2	γ_3	$\overline{\gamma}$	κ
GaAs	6.85	2.1	2.9	2.58	1.2
InAs	20.4	8.3	9.1	8.78	7.6

The effective 2D Hamiltonian depends only on 2D variables, i.e., it cannot contain z, p_z, and A_z. We assume that the gate lateral potential is smooth enough, $\nabla U \ll kU$, so we can use the gradient expansion of the potential. As soon as we understand this point, the kinematic form of the 2D Hamiltonian is unambiguously dictated by symmetries:

$$\begin{aligned} H_{2D} = {} & \varepsilon(\boldsymbol{\pi}) + U(x,y) \\ & + \{\alpha(\boldsymbol{\pi}), (\boldsymbol{s}\cdot[\nabla U \times \boldsymbol{\pi}])\} + \frac{1}{2}\{\beta(\boldsymbol{\pi}), \Delta U\} \\ & - g_{zz}(\boldsymbol{\pi})\mu_B B_z s_z \\ & - \frac{\mu_B}{2}\overline{g}_1(\boldsymbol{\pi})(B_+\pi_+^2 s_- + B_-\pi_-^2 s_+) \\ & - \frac{\mu_B}{2}\overline{g}_2(\boldsymbol{\pi})(B_-\pi_+^4 s_- + B_+\pi_-^4 s_+). \end{aligned} \tag{10}$$

Here, $\mathbf{s} = \boldsymbol{\sigma}/2$ is the pseudospin, $B_\pm$, $\pi_\pm$, and $s_\pm$ are standard ladder operators, $B_\pm = B_x \pm iB_y$, etc., and $\{\ldots\}$ is the anticommutator. We stress again that all the variables, gradients, etc. in the Hamiltonian are two dimensional. While the dispersion $\varepsilon(k)$ has been discussed in the previous section, the functions $\alpha(k)$, $\beta(k)$, $g_{zz}(k)$, $\overline{g}_1(k)$, and $\overline{g}_2(k)$ will be determined in subsequent sections. Like the dispersion, they are isotropic, i.e., depend on $k = |\boldsymbol{k}|$. When determining the kinematic form of the Hamiltonian (10) one has to remember that it has to respect (i) symmetry with respect to rotations around the z axis, (ii) gauge invariance, (iii) time-reversal symmetry, (iv) to be parity even, and (v) to be invariant under the transformation $x \to x$, $y \to -y$. The first two terms in Eq. (10) are standard ones and do not require comments. One can say that the α term and the β term are textbook spin-orbit and Darwin terms. Since both ∇U and $\boldsymbol{\pi}$ have only in-plane components, only s_z contributes in the α term. The g_{zz} term is the usual Zeeman interaction which respects all the symmetries. The spiral representation is convenient to determine the response to the in-plane magnetic field. The ladder operator s_+ changes the projection of real spin by $\Delta S_z = 3$. Hence, under rotation of the coordinate system around the z axis by angle ϕ, the operator s_+ is transformed as $s_+ \to s_+ e^{3i\phi}$. Both $\boldsymbol{B}$ and $\boldsymbol{\pi}$ are the usual vectors, so $B_+ \to B_+ e^{i\phi}$, $\pi_+ \to \pi_+ e^{i\phi}$. There are only two kinematic structures bilinear in $B_\pm$ and $s_\pm$ that do not change under the rotation. These are the $\overline{g}_1$ and $\overline{g}_2$ structures in Eq. (10). Due to reflection symmetry, $x \to x$, $y \to -y$, both $\overline{g}_1$ and $\overline{g}_2$ are real.

It is useful to underline the most important points concerning Eq. (10). (i) This is a gradient expansion up to the second gradient of U; we neglect third derivatives of the gate potential. The Darwin term, $\propto \Delta U$, is spin independent. We keep it for completeness because, as in the Dirac equation, it comes together with the usual spin orbit and the coefficients α and β have the same dimensions. (ii) Due to the gauge invariance, all

the coefficients α, β, g_{zz}, $\overline{g}_1$, and $\overline{g}_2$ depend on the kinematic momentum $\boldsymbol{\pi} = \boldsymbol{k} - e\boldsymbol{A}$, where $\boldsymbol{A}$ depends only on x and y and, hence, describes only the z component of the magnetic field. (iii) The α and β terms contain anticommutators. (iv) We neglect powers of magnetic field higher than one in the spin response; for example, we neglect the kinematic structures such as $B_+^3 s_-$. However, it is possible to restore these terms with the developed technique.

Now we proceed to the calculation of functions which enter the effective Hamiltonian (10). We start from the in-plane g-factors.

IV. IN-PLANE g-FACTORS

There are two independent in-plane g-functions: $\overline{g}_1(k)$ and $\overline{g}_2(k)$; see Eq. (10). To find these functions, we numerically diagonalize the Luttinger Hamiltonian (9) with $U = 0$ and with the magnetic field directed along the x axis, $\boldsymbol{B} = (B,0,0)$. We use the vector potential in the following gauge:

$$\mathbf{A} = (0, -Bz, 0). \tag{11}$$

In this gauge, the in-plane momentum $\boldsymbol{k}$ is a good quantum number, $\psi \propto e^{ik_x x + ik_y y}$. Therefore $\boldsymbol{k}$ enters Eq. (9) as a simple number, so only the one-dimensional z-confinement problem needs to be diagonalized numerically. We calculate the magnetic spin-splitting of the HH1 subband at different values of $\boldsymbol{k}$. Because we have to find two different functions, we perform calculation twice with $\boldsymbol{k} = (k,0)$ and with $\boldsymbol{k} = (0,k)$. Effective momentum-dependent g-factors

$$\begin{aligned} g_1 &= k^2 \overline{g}_1(k), \\ g_2 &= k^4 \overline{g}_2(k) \end{aligned} \tag{12}$$

for GaAs and InAs and for parabolic and rectangular quantum wells are plotted in Fig. 4.

At small k, the g-factors (12) scale as high powers of momentum. Therefore, it is instructive to plot also $\overline{g}_1$ and $\overline{g}_2$. These functions have dimensions $[1/k^2]$ and $[1/k^4]$, respectively. We use powers of k_0 [Eq. (7)] to balance the momentum dimension. Plots of $k_0^2 \overline{g}_1(k)$ and $k_0^4 \overline{g}_2(k)$ are presented in Fig. 5. The zero-momentum value of $\overline{g}_1$ can be calculated analytically with the usual perturbation theory. The result reads

$$\begin{aligned} \overline{g}_1(0) &= -3\overline{\gamma}(\kappa Z_1 - 4\overline{\gamma} Z_2 - \overline{\gamma} Z_3 + 2\kappa\overline{\gamma} Z_4), \\ Z_1 &= -2\sum_{n=1}^{\infty} \frac{|\langle 1H|nL\rangle|^2}{m(\varepsilon_{nL} - \varepsilon_{1H})}, \\ Z_2 &= 2i\sum_{n=1}^{\infty} \frac{\langle 1H|z|nL\rangle\langle nL|p_z|1H\rangle}{m(\varepsilon_{nL} - \varepsilon_{1H})}, \\ Z_3 &= -2i\sum_{n=1}^{\infty} \frac{\langle 1H|\{z,p_z\}|nL\rangle\langle nL|1H\rangle}{m(\varepsilon_{nL} - \varepsilon_{1H})}, \\ Z_4 &= 2\sum_{n=1}^{\infty} \frac{|\langle 1H|p_z|nL\rangle|^2}{m^2(\varepsilon_{nL} - \varepsilon_{1H})^2}. \end{aligned} \tag{13}$$

The zero-momentum value of $\overline{g}_1$ has been calculated in Ref. [13] with only Z_1 and Z_2 terms taken into account. The Z_4 term is not important; it is always much smaller than the other terms because it comes from third-order perturbation theory. We present the term only because it has no a formal parametric suppression compared with other terms. However the Z_3 term is generally important. Due to this term our values of $\overline{g}_1(0)$ differ from that of Ref. [13] for a parabolic well. Values corresponding to Ref. [13] are shown in Fig. 5 by red dots. Accidentally, Z_3 is zero for an infinite rectangular quantum well because in this case $\langle nL|1H\rangle = \delta_{n1}$ and $\langle 1H|\{z,p_z\}|1H\rangle = 0$.

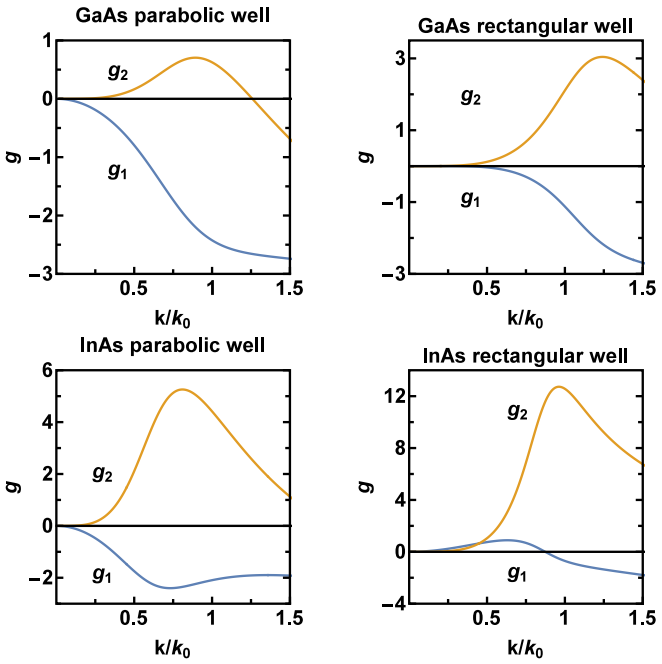

FIG. 4. Effective in-plane HH1 g-factors [see Eq. (12)] versus momentum. The g-factors are presented for parabolic and rectangular confinement in GaAs and InAs.

The most important conclusion of this section is that, at $k \approx k_0$ where most experiments are performed, both invariant g-factors g_1 and g_2 are equally important; see Fig. 4.

V. SPIN-ORBIT INTERACTION DUE TO LATERAL GATE POTENTIAL

To calculate the spin-orbit interaction and the Darwin term in the effective Hamiltonian (10) we employ the scattering amplitude method which is usually used for derivation of the Breit interaction in quantum electrodynamics [31]. This is a technically efficient way to proceed from a full multicomponent description to the effective two-component wave function. The magnetic field is not relevant to this problem, so in this section the magnetic field is zero. Consider scattering of a hole from a weak lateral potential limited in space. The actual shape of the potential is not important, the only important point is that the potential is weak and limited in space, so the scattering problem makes sense. The idea of the method is to calculate the Born scattering amplitude, $\boldsymbol{k} \to \boldsymbol{k}'$. The scattering amplitude calculated with the effective Hamiltonian (10) must be the same as the amplitude calculated with the 3D Hamiltonian (9). This allows one to find functions $\alpha(k)$ and $\beta(k)$ in Eq. (10).

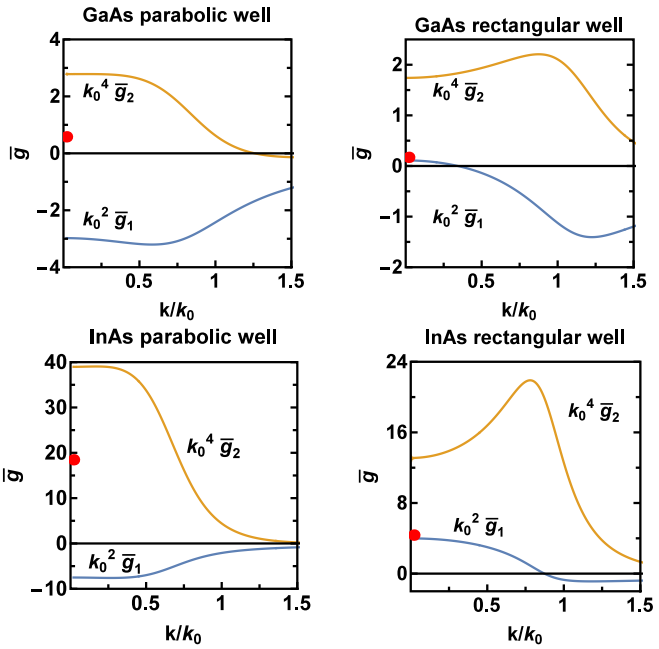

FIG. 5. Functions $\bar{g}_1(k)$ and $\bar{g}_2(k)$ related to the in-plane g-factors; see Eq. (12). The functions are presented for parabolic and rectangular quantum wells in GaAs and InAs. To balance dimensions, we plot the functions multiplied by a corresponding power of k_0. Red points on the vertical axes indicate the values of $\bar{g}_1(k=0)$ calculated by using equations in Ref. [13]. The points must be compared with our blue lines.

An eigenstate of the Hamiltonian (5), $|S_z,n,\boldsymbol{k}\rangle$, possesses a definite value of the in-plane momentum $\boldsymbol{k}$ and a definite value of $S_z = -3/2,\ -1/2,\ 1/2,\ 3/2$,

$$|S_z,n,\boldsymbol{k}\rangle = e^{i\boldsymbol{k}\cdot\boldsymbol{r}}|S_z,n\rangle. \tag{14}$$

Here, the index n enumerates transverse modes (z standing waves). Diagonalization of the Hamiltonian (6), which is described in Sec. II, results in energy bands and in wave functions expressed in terms of Eq. (14). In particular, the wave function $|\uparrow,\boldsymbol{k}\rangle$ of the HH1 band is of the form

$$|\uparrow,\boldsymbol{k}\rangle = e^{ikr}\sum_{S_z} k_+^{(3/2-S_z)}\sum_n a_n(S_z,k)|S_z,n\rangle, \tag{15}$$

where the momentum-dependent coefficients $a_n(S_z,k)$ are determined by the numerical diagonalization of the 3D Luttinger Hamiltonian with $U(x,y)=0$. The phase factor, $k_+^{(3/2-S_z)}$ is dictated by the conservation of the total angular momentum.

To understand Eq. (15) note that, at $k\to 0$, Eq. (15) contains only one term which has $S_z = 3/2$ because in this limit $|\uparrow\rangle = |S_z = 3/2\rangle$. Account of the spin nondiagonal perturbation V (6), proportional to the in-plane momentum, admixes other values of S_z to the wave function. For example, the leading order in V gives us terms $\propto k_+|S_z = 1/2\rangle$ and $\propto k_+^2|S_z = -1/2\rangle$; see Ref. [30]. The power of k_+ reflects conservation of angular momentum, $3/2 = 1+1/2 = 2-1/2$. It is obvious that conservation of angular momentum is valid in any order of perturbation theory. This determines the angular structure of the wave function (15) reflected in the factor $k_+^{(3/2-S_z)}$.

The Born scattering amplitude is given by the matrix element of the scattering potential U between the initial and final states,

$$f_{\mathbf{k}'\mathbf{k}} = \langle\uparrow,\boldsymbol{k}'|U(\mathbf{r})|\uparrow,\boldsymbol{k}\rangle = U_{\mathbf{q}}\sum_{l=0}^{3} b_l(k)(k'_-k_+)^l, \tag{16}$$

where

$$b_l(k) = \sum_{n=1}^{\infty}\left|a_n\left(\frac{3}{2}-l,k\right)\right|^2, \tag{17}$$

U_q is the Fourier transform of $U(\mathbf{r})$, and $\boldsymbol{q} = \mathbf{k}'-\mathbf{k}$ is the momentum transfer. When calculating Eq. (16) by using Eq. (15), we take into account that $\mathbf{k}'^2 = \mathbf{k}^2$ due to the energy conservation. Note that the wave-function normalization condition reads

$$1 = b_0 + k^2 b_1 + k^4 b_2 + k^6 b_3. \tag{18}$$

There is no spin-flip scattering, $\langle\uparrow,\boldsymbol{k}'|U(\mathbf{r})|\downarrow,\boldsymbol{k}\rangle = 0$, due to P-parity conservation for symmetric heterostructures. Because the gradient expansion coefficients do not depend on the in-plane confinement, we may consider the symmetric one. Then, the wave function (15) and its time-reversed counterpart give us the odd power of momentum variables $\mathbf{k}$ and $\mathbf{k}'$ which makes the spin-flip part of the scattering amplitude P-odd. However, the spin-flip scattering appears in asymmetric heterostructures where P-parity is violated.

The product k'_-k_+ which enters Eq. (16) reads

$$k'_-k_+ = k^2 - \tfrac{1}{2}q^2 + i[q_x k_y - q_y k_x]. \tag{19}$$

The first power of the square bracket in this equation is responsible for the skew scattering. Therefore, comparing the $[\boldsymbol{q}\times\boldsymbol{k}]$ term from Eq. (16) with the scattering amplitude calculated with the α term in Eq. (10) we find the following expression for α:

$$\alpha(k) = b_1(k) + 2k^2 b_2(k) + 3k^4 b_3(k). \tag{20}$$

Similarly, the terms proportional to q^2 in Eq. (16) contribute to the Darwin term. Comparing the q^2 term from Eq. (16) with the scattering amplitude calculated with the β term in Eq. (10) we find the following expression for β:

$$\beta(k) = \tfrac{1}{2}b_1(k) + 2k^2 b_2(k) + \tfrac{9}{2}k^4 b_3(k). \tag{21}$$

There are also higher powers of q in Eq. (16), up to q^6; they correspond to higher gradients in the gradient expansion of the effective Hamiltonian. We can neglect the higher gradients in Eq. (10) by assuming that U is sufficiently smooth. However, in principle, the scattering amplitude method (16) allows us to find all the terms of the gradient expansion.

Since the numerical diagonalization described in Sec. II gives all coefficients of the HH1 wave function, it is easy to calculate α and β by using Eqs. (17), (20), and (21). Functions $\alpha(k)$ and $\beta(k)$ for parabolic and rectangular quantum wells in GaAs and InAs are plotted in Fig. 6. Both α and β have dimension $[1/k^2]$. To balance the dimension in Fig. 6, we plot $k_0^2\alpha$ and $k_0^2\beta$.

Since we consider a symmetric quantum well there is no Rashba interaction related to the well asymmetry. Nevertheless, there is an intrinsic band-structure spin-orbit interaction

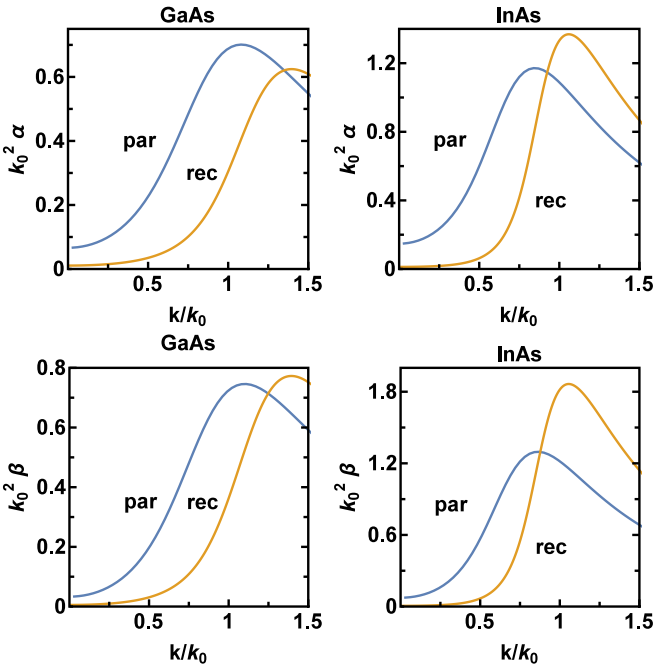

FIG. 6. The spin-orbit α and the Darwin β functions for the lateral gate potential, see Eq. (10). The functions are presented for parabolic and rectangular quantum wells in GaAs and InAs and multiplied by powers of k_0 to make them dimensionless.

which has the same kinematic form as the α term in Eq. (10) and which sometimes is called the intrinsic Rashba SOI, $H_R \sim -r_{41}^{8v8v}[\nabla U \times \boldsymbol{k}]\boldsymbol{S}$. Here S is the hole spin $\frac{3}{2}$. We use notations of Ref. [7]. In GaAs the coefficient is $r_{41}^{8v8v} \approx -15\text{Å}^2$; see Ref. [7]. To compare the α term and the intrinsic Rashba SOI we take parameters corresponding to typical experimental conditions, $d = 15$ nm, $k = k_0$. It is easy to check that in this situation the α term in Eq. (10) is about 80 times larger than the intrinsic Rashba SOI.

While the Darwin term in Eq. (10) is theoretically important, it is hard to suggest an experiment to directly measure this term. Let us consider as an example a quantum dot with potential $U = U_0 + m^*\omega^2(x^2 + y^2)/2$. In this case, the Darwin term effectively shifts the ground, $U_0 \to U_0 + \delta U_0$, $\delta U_0 = 2\beta m^*\omega^2$. The change can be sizable, at $\omega = 0.5$ meV the shift is $\delta U_0 \lesssim 0.1$ meV. However, it is not clear how to directly measure or control the value of U_0. The usual Dirac-equation Darwin term is measured via the energy shift of s-wave electron levels in the hydrogen atom. In principle, such a measurement is possible in our case too with an acceptor in the 2D heterostructure. The acceptor creates the attractive potential $U \propto -1/r$, $r \gg d$, and due to the Darwin term there is a perturbation $\delta U \propto -1/r^3$ that shifts hole levels compared with the simple Coulomb field. This term provides a big energy shift δE_s for s waves enhanced by the power-law divergence of the integral $\delta E_s \propto \int \Psi_s^2(r)\Delta U d^2r \propto \int \Psi_s^2(r)dr/r^2$ at small $r \sim d$ because $\Psi_s^2(r=0) \neq 0$, where $\Psi_s(r)$ is the wave function of the s mode. There is no such divergence for other modes. Hence, the Darwin term may result in significant energy shifts of s-wave levels in the 2D acceptor spectrum.

VI. OUT-OF-PLANE g-FACTOR

A naive value of g_{zz} is $g_{zz} = 6\kappa$; see Eq. (9) and Ref. [7]. Virtual orbital 3D dynamics strongly influences this value. The effect of the virtual dynamics at $k = 0$ has been calculated previously; it leads to a very significant reduction of the g-factor [24–27]:

$$g_{zz}(0) = 6\kappa - 12\overline{\gamma}^2 \sum_{n=1}^{\infty} \frac{|\langle 1H|p_z|nL\rangle|^2}{m(\varepsilon_{nL} - \varepsilon_{1H})}. \tag{22}$$

The g-factor is significantly different from the naive value. For example, the g-factor in GaAs, where $6\kappa = 7.2$, is $g_{zz}(0) = 7.2 - 5.15 = 2.05$ for a parabolic quantum well and $g_{zz}(0) = 7.2 - 2.6 = 4.6$ for a rectangular quantum well. Our goal in this section is to calculate the entire function $g_{zz}(k)$ defined in Eq. (10). One possibility is to calculate Landau levels with the Hamiltonian (9) and then look at the spin splitting of the levels. This approach, used in Ref. [27] for the rectangular well, indicated a significant dependence of the g-factor on Landau level. However, this method is rather technically involved and computationally expensive. Here we use a different method, we destroy Landau levels by a gate potential and calculate the linear spin response.

Let us consider the parabolic gate potential

$$U(x) = \frac{m\omega_x^2 x^2}{2}, \tag{23}$$

which restricts the hole propagation in the x direction. The vector potential for the out-of-plane magnetic field $\boldsymbol{B} = (0,0,B)$ is taken in the following gauge:

$$\mathbf{A} = (0, Bx, 0). \tag{24}$$

So, the y component of momentum is conserved and we set $k_y = 0$. In this situation, the long momentum that enters the full Luttinger Hamiltonian (9) is $\boldsymbol{\pi} = (p_x, -eBx, p_z)$. Since there is no dynamics along the y direction, $e^{ik_y y} = 1$, effectively the Hamiltonian (9) becomes two dimensional; only the x and the z directions are nontrivial. A brute force numerical diagonalization of this Hamiltonian is straightforward. We consider energy below the bottom of the first-excited band; see Fig. 2, so all quantum states we consider originate from the lowest HH1 band. Due to the gate confinement (23), the spectrum is discrete; it is described by an integer quantum number $n_x = 1,2,3,\ldots$ and, due to the magnetic field, the Kramers degeneracy of each n_x level is lifted, as illustrated in Fig. 7. For numerical calculations with Eqs. (9) and (23), we use sufficiently small values of ω_x, $\omega_x \sim 0.01$, so that there are about 100–150 oscillator levels within the energy span of the HH1 band. It is worth noting that the spectrum is not equidistant because the dispersion $\varepsilon(p)$ is not parabolic. The magnetic field which we consider in this analysis is even smaller than ω_x, $B \ll \omega_x$. In practice, we first diagonalize Eqs. (9) and (23) numerically at $B = 0$, and then we account for the weak magnetic field by the usual perturbation theory. As result, we find the Zeeman splitting of each oscillator level; see Fig. 7,

$$\Delta\varepsilon = -g(\varepsilon)\tfrac{1}{2}\mu_B B\sigma_z. \tag{25}$$

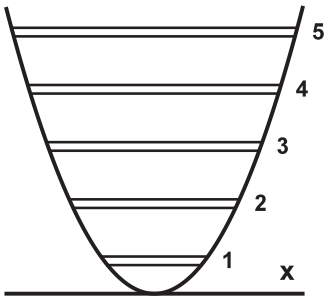

FIG. 7. Magnetic-field split oscillator levels with $n_x = 1,2,3,\ldots$ in the parabolic gate potential (23).

Here, ε is energy corresponding to the oscillator level with quantum number n_x. The outcome of the brute force numerical calculation is the function $g(\varepsilon)$.

The next question is how to deduce the function $g_{zz}(k)$ in Eq. (10) from $g(\varepsilon)$ obtained in the numerical calculation described in the previous paragraph? To answer this question, let us articulate the problem in terms of the effective 2D Hamiltonian (10). With the gate potential (23) the effective Hamiltonian takes the following form:

$$H_{2D} = \varepsilon(k_x) + \frac{m\omega_x^2}{2}(x^2 + 2\beta) - \left[g_{zz} + 2m^2\omega_x^2\{\alpha,x^2\}\right]\frac{1}{2}\mu_B B\sigma_z. \quad (26)$$

Actually, the Hamiltonian becomes one dimensional (1D). Recall that $\alpha(k_x)$ is the coefficient in the gate spin-orbit interaction and $\beta(k_x)$ is the coefficient in the gate Darwin term, both functions have been determined in Sec. V. The α term in Eq. (26) is due to $\pi_y = -eBx$. Equation (26) is written within linear in B approximation; we neglect $\pi_y^2 = (eBx)^2$ which is quadratic in B. There is an important point to note about the Hamiltonian (26): the Zeeman splitting arises not only due to g_{zz}—there is a part of the splitting which is due to the gate potential. This point is important for understanding experiments with quantum point contacts and quantum dots in an out-of-plane magnetic field.

Let us set $B = 0$ in Eq. (26):

$$H_{2D}^{(0)} = \varepsilon(k_x) + \frac{m\omega_x^2}{2}(x^2 + 2\beta). \quad (27)$$

In the semiclassical limit, $n_x \gg 1$, Eq. (27) determines x^2 as function of k_x at a given energy ε:

$$x^2 = \frac{2}{m\omega_x^2}[\varepsilon - \overline{\varepsilon}(k_x)],$$
$$\overline{\varepsilon}(k_x) = \varepsilon(k_x) + m\omega_x^2\beta(k_x). \quad (28)$$

Here ε is the eigenenergy of the state with quantum number n_x. The ω_x^2 term in Eq. (28) can be safely neglected, so $\overline{\varepsilon}(k_x) \approx \varepsilon(k_x)$. Hamiltonian (27) depends quadratically on x, therefore, having in mind the interchange $k_x \to x$, $x \to k_x$, it is easy to find the semiclassical eigenfunction of Eq. (27) in the momentum representation:

$$\Psi^2(k_x,\varepsilon) = \frac{1}{N(\varepsilon)\sqrt{\varepsilon - \overline{\varepsilon}(k_x)}}. \quad (29)$$

The eigenenergy ε is determined by the Bohr–Sommerfeld quantization condition

$$4 \times \sqrt{\frac{2}{m\omega_x^2}} \int_0^{k_{\max}} \sqrt{\varepsilon - \overline{\varepsilon}(k_x)}dk_x = 2\pi n_x, \quad (30)$$

where $k_{\max}$ is the turning point in the momentum space, $\overline{\varepsilon}(k_{\max}) = \varepsilon$. The normalization coefficient in Eq. (29) is

$$N(\varepsilon) = \int_0^{k_{\max}} \frac{dk_x}{\sqrt{\varepsilon - \overline{\varepsilon}(k_x)}}. \quad (31)$$

This normalization assumes that the momentum in Eq. (29) is always positive, $k_x > 0$.

The Zeeman splitting of the oscillator level is given by usual perturbation theory with wave function (29) and with the B term in Eq. (26) being the perturbation:

$$g(\varepsilon) = \int_0^{k_{\max}} \Psi^2(k_x,\varepsilon)[g_{zz}(k_x) + g_\alpha(k_x)]dk_x,$$
$$g_\alpha(k_x) = 4m^2\omega_x^2\alpha(k_x)x^2(k_x), \quad (32)$$

where $x^2(k_x)$ is defined by Eq. (28). We know the function $g(\varepsilon)$ from the numerical diagonalization of the 3D Luttinger Hamiltonian; see Eq. (25). Functions $\Psi(k_x,\varepsilon)$, $\alpha(k_x)$, and $x(k_x)$ have been already calculated. In the next paragraph we explain how to invert the integral equation (32) to find the function $g_{zz}(k_x)$.

To solve the integral equation (32) we use a well-known mathematical method developed in classical mechanics for the purpose of determining a potential in terms of a known period of motion [36]. Here we briefly describe the method. We can rewrite Eq. (32) as

$$f(\varepsilon) = \int_0^{k_{\max}} \frac{g_{zz}(k_x)dk_x}{\sqrt{\varepsilon - \overline{\varepsilon}(k_x)}}, \quad (33)$$

where

$$f(\varepsilon) = N(\varepsilon)\left(g(\varepsilon) - \int_0^{k_{\max}} \Psi^2(k_x,\varepsilon)g_\alpha(k_x)dk_x\right) \quad (34)$$

is a known function. Changing the integration variable we transform Eq. (33) to

$$f(\varepsilon) = \int_0^{\varepsilon} \frac{h(\overline{\varepsilon})d\overline{\varepsilon}}{\sqrt{\varepsilon - \overline{\varepsilon}}}, \quad (35)$$

where

$$h(\overline{\varepsilon}) = \frac{g_{zz}(k(\overline{\varepsilon}))}{v(\overline{\varepsilon})}, \quad (36)$$

and $v(\overline{\varepsilon}) = \partial\overline{\varepsilon}(k)/\partial k$ is the velocity. Next we integrate Eq. (35) over ε with the kernel $1/\sqrt{\eta - \varepsilon}$, where η is an external energy

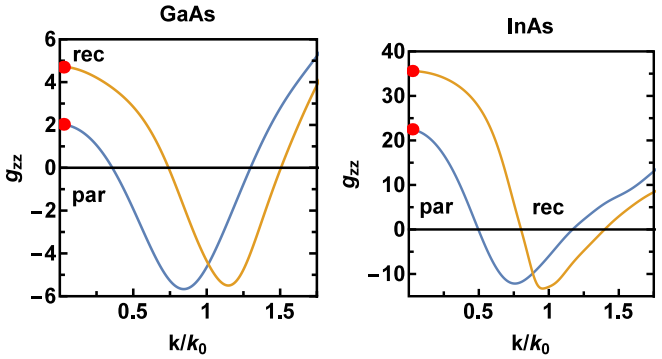

FIG. 8. Out-of-plane g-factor g_{zz} as function of the in-plane momentum. The g-factor is presented for parabolic and rectangular quantum wells in GaAs and InAs. Red dots show values of g_{zz} at $k = 0$ obtained with Eq. (22).

variable:

$$\int_0^\eta \frac{f(\varepsilon)d\varepsilon}{\sqrt{\eta-\varepsilon}} = \int_0^\eta \int_0^\varepsilon \frac{h(\bar{\varepsilon})d\bar{\varepsilon}d\varepsilon}{\sqrt{\eta-\varepsilon}\sqrt{\varepsilon-\bar{\varepsilon}}} = \pi \int_0^\eta h(\varepsilon)d\varepsilon. \quad (37)$$

Finally, differentiating Eq. (37) over η, we find the function $g_{zz}(k)$:

$$g_{zz}(k) = \frac{v(\eta)}{2\pi\sqrt{\eta}} \int_0^1 [f(\eta y) + 2\eta y f'(\eta y)] \frac{dy}{\sqrt{1-y}}, \quad (38)$$

where η and k are related as $\eta = \bar{\varepsilon}(k)$.

Equation (38) solves the inverse problem. So, having the result (25) of the numerical diagonalization of the 3D Luttinger Hamiltonian and using Eq. (38), we find the out-of-plane g-factor. Plots of $g_{zz}(k)$ for parabolic and rectangular quantum wells in GaAs and InAs are presented in Fig. 8. Values of g_{zz} at $k = 0$ obtained with Eq. (22) are shown in Fig. 8 by red dots.

Typical experimental densities correspond to the range of in-plane momentum k from $0.5k_0$ to $1.5k_0$. According to Fig. 8, this region contains two points where g_{zz} changes its sign and these points can be achieved experimentally. The absolute value $|g_{zz}| \approx 5$ at $k \approx k_0$ is consistent with experimental data; see Refs. [13,14].

VII. CONCLUSIONS

We perform the 3D → 2D dimensional reduction of the Luttinger Hamiltonian for holes in zinc-blende semiconductors in the presence of a symmetric quantum well, a smooth lateral gate potential, and an uniform external magnetic field. Our results are applicable to all kinds of two-dimensional symmetric semiconductor heterostructures. The effective 2D Hamiltonian (10) is written as a Ginzburg–Landau-type gradient expansion in gradients of the lateral potential. We develop general methods and techniques to calculate parameters of the effective Hamiltonian as functions of the hole momentum. We specifically present numerical results for the parabolic quantum well and for the infinite rectangular quantum well in GaAs and InAs. In the paper we obtain the following results: (i) We develop the method of calculation and calculate g-factors for the in-plane direction of the magnetic field. In particular, we point out that there are two kinematically different g-factors, g_1 and g_2. An important consequence of two different g-factors is the anisotropic magnetic response in the presence of an anisotropic lateral gate potential. The g-factors as functions of the hole momentum are plotted in Fig. 4. (ii) We develop the method of calculation and calculate the spin-orbit interaction and the Darwin interaction related to the lateral gate potential. The functions α (spin-orbit) and β (Darwin) are plotted in Fig. 6 versus the hole momentum. (iii) We develop the method of calculation and calculate the g_{zz}-factor for the out-of-plane direction of the magnetic field. We also point out that, in the presence of a gate potential (quantum point contact or quantum dot), the magnetic response is not only due to g_{zz}—there is a part of the response related to the gate potential which is also calculated. The plot of g_{zz} versus momentum is presented in Fig. 8.

ACKNOWLEDGMENTS

We thank A. Hamilton and A. Srinivasan for stimulating discussions and interest in the work. We are also grateful to L. E. Golub and U. Züelicke for valuable communications. The work has been supported by the Australian Research Council Grant No. DP160103630.

[1] G. Dresselhaus, Phys. Rev. **100**, 580 (1955).
[2] Yu. A. Bychkov and E. I. Rashba, Sov. Phys. JETP Lett. **39**, 78 (1984).
[3] R. L. Kallaher, J. J. Heremans, N. Goel, S. J. Chung, and M. B. Santos, Phys. Rev. B **81**, 075303 (2010).
[4] J. P. Heida, B. J. van Wees, J. J. Kuipers, T. M. Klapwijk, and G. Borghs, Phys. Rev. B **57**, 11911 (1998).
[5] J. M. Luttinger, Phys. Rev. **102**, 1030 (1956).
[6] M. Cardona, N. E. Christensen, and G. Fasol, Phys. Rev. B **38**, 1806 (1988).
[7] R. Winkler, *Spin-Orbit Coupling Effects in Two-Dimensional Electron and Hole Systems* (Springer-Verlag, Berlin, Heidelberg, 2003).
[8] T. Li, L. A. Yeoh, A. Srinivasan, O. Klochan, D. A. Ritchie, M. Y. Simmons, O. P. Sushkov, and A. R. Hamilton, Phys. Rev. B **93**, 205424 (2016).
[9] R. Danneau, O. Klochan, W. R. Clarke, L. H. Ho, A. P. Micolich, M. Y. Simmons, A. R. Hamilton, M. Pepper, D. A. Ritchie, and U. Züelicke, Phys. Rev. Lett. **97**, 026403 (2006).
[10] S. P. Koduvayur, L. P. Rokhinson, D. C. Tsui, L. N. Pfeiffer, and K. W. West, Phys. Rev. Lett. **100**, 126401 (2008).
[11] O. Klochan, A. P. Micolich, L. H. Ho, A. R. Hamilton, K. Muraki, and Y. Hirayama, New J. Phys. **11**, 043018 (2009).
[12] J. C. H. Chen, O. Klochan, A. P. Micolich, A. R. Hamilton, T. P. Martin, L. H. Ho, U. Züelicke, D. Reuter, and A. D. Wieck, New J. Phys. **12**, 033043 (2010).
[13] Y. Komijani, M. Csontos, I. Shorubalko, U. Züelicke, T. Ihn, K. Ensslin, D. Reuter, and A. D. Wieck, Europhys. Lett. **102**, 37002 (2013).
[14] A. Srinivasan, L. A. Yeoh, O. Klochan, T. P. Martin, J. C. H. Chen, A. P. Micolich, A. R. Hamilton, D. Reuter, and A. D. Wieck, Nano Lett. **13**, 148 (2013).

[15] F. Nichele, S. Chesi, S. Hennel, A. Wittmann, C. Gerl, W. Wegscheider, D. Loss, T. Ihn, and K. Ensslin, Phys. Rev. Lett. **113**, 046801 (2014).
[16] V. A. Kulbachinskii, P. V. Gurin, O. V. Vikhrova, Yu. A. Danilov, and B. N. Zvonkov, J. Phys.: Conf. Ser. **100**, 042025 (2008).
[17] C. D. Cress, C. G. Bailey, S. M. Hubbard, D. M. Wilt, S. G. Bailey, and R. P. Raffaelle, *Proceedings of the 33rd IEEE Photovoltaics Specialists Conference* (IEEE, New York, 2008).
[18] O. Klochan, A. P. Micolich, A. R. Hamilton, K. Trunov, D. Reuter, and A. D. Wieck, Phys. Rev. Lett. **107**, 076805 (2011).
[19] D. V. Bulaev and D. Loss, Phys. Rev. Lett. **98**, 097202 (2007).
[20] L. A. Yeoh, A. Srinivasan, O. Klochan, R. Winkler, U. Züelicke, M. Y. Simmons, D. A. Ritchie, M. Pepper, and A. R. Hamilton, Phys. Rev. Lett. **113**, 236401 (2014).
[21] E. Bangert and G. Landwehr, Surf. Sci. **170**, 593 (1986).
[22] R. Winkler, M. Merkler, T. Darnhofer, and U. Rössler, Phys. Rev. B **53**, 10858 (1996).
[23] M. Failla, M. Myronov, C. Morrison, D. R. Leadley, and J. Lloyd-Hughes, Phys. Rev. B **92**, 045303 (2015).
[24] Th. Wimbauer, K. Oettinger, Al. L. Efros, B. K. Meyer, and H. Brugger, Phys. Rev. B **50**, 8889 (1994).
[25] M. V. Durnev, M. M. Glazov, E. L. Ivchenko, M. Jo, T. Mano, T. Kuroda, K. Sakoda, S. Kunz, G. Sallen, L. Bouet, X. Marie, D. Lagarde, T. Amand, and B. Urbaszek, Phys. Rev. B **87**, 085315 (2013).
[26] I. L. Drichko, V. A. Malysh, I. Yu. Smirnov, L. E. Golub, S. A. Tarasenko, A. V. Suslov, O. A. Mironov, M. Kummer, and H. von Känel, Phys. Rev. B **90**, 125436 (2014).
[27] G. E. Simion and Y. B. Lyanda-Geller, Phys. Rev. B **90**, 195410 (2014).
[28] C. Gradl, M. Kempf, D. Schuh, D. Bougeard, R. Winkler, C. Schüller, and T. Korn, Phys. Rev. B **90**, 165439 (2014).
[29] L. C. Andreani, A. Pasquarello, and F. Bassani, Phys. Rev. B **36**, 5887 (1987).
[30] O. P. Sushkov and A. H. Castro Neto, Phys. Rev. Lett. **110**, 186601 (2013).
[31] V. B. Berestetskii, E. M. Lifshitz, and L. P. Pitaevskii, *Quantum Electrodynamics* (Pergamon Press, Oxford, 1982).
[32] A. Baldereschi and N. O. Lipari, Phys. Rev. B **8**, 2697 (1973).
[33] R. Winkler, S. J. Papadakis, E. P. De Poortere, and M. Shayegan, Phys. Rev. Lett. **85**, 4574 (2000).
[34] R. Winkler, D. Culcer, S. J. Papadakis, B. Habib, and M. Shayegan, Semicond. Sci. Technol. **23**, 114017 (2008).
[35] D. S. Miserev, A. Srinivasan, I. Farrer, D. A. Ritchie, A. R. Hamilton, and O. P. Sushkov, arXiv:1612.00572v1.
[36] L. D. Landau and E. M. Lifshitz, *Mechanics*, A Course of Theoretical Physics Vol. 1 (Pergamon Press, Oxford, 1969).